MADRID
inter.noise 2019
June 16 - 19
NOISE CONTROL FOR A BETTER ENVIRONMENT

An Inverse Method to Determine Acoustic Parameters of Polyurethane Foams

Dossi, Martino[1]
Brennan, Mark[2]
Moesen, Maarten[3]
Vandenbroeck, Jan[4]
Huntsman Polyurethanes
Everslaan 45, 3078 Everberg, Belgium

Huo, Lisha[5]
Department of Materials Engineering, Catholic University of Leuven (KU Leuven)
Kasteelpark Arenberg 44, 3001 Leuven, Belgium

ABSTRACT

Polyurethane (PU) foams are widely used as noise and vibration damping materials in automobile applications. Their porous random microstructure is composed of a visco-elastic frame structure with an interstitial fluid filling the voids. Acoustic and mechanical energy absorption properties and their direct link with microstructure morphology are therefore of paramount importance in the design, prediction and optimisation of the material behaviour. Although some parameters can be directly measured, the complete acoustic characterisation of porous materials remains a real challenge.

For that reason, an inverse calculation of acoustic parameters based on impedance tube measurement is proposed. Equivalent fluid models are used to study the wave propagation process within PU rigid foams, in which acoustic properties depend on the effective density and bulk modulus of the fluid. Conversely, Biot poroelastic model is used to study the multi-physical coupling between mechanical vibrations of the solid structure and acoustic waves in the fluid. Biot coupling is often present in the wave propagation through PU flexible foams, having a soft-like polymeric structure and semi-open microstructure. Finally, the macroscopic properties obtained by inverse numerical modelling are then linked to polymer characterisation obtained by Dynamical Mechanical Analysis and the material microstructure obtained with µCT.

Keywords: Sound Absorbing Porous Materials, Noise Vibration and Harshness (NVH), Polyurethanes
I-INCE Classification of Subject Number: 35, 47, 76

[1] martino_dossi@huntsman.com
[2] mark_brennan@huntsman.com
[3] maarten_moesen@huntsman.com
[4] jan_vandenbroeck@huntsman.com
[5] lisha.huo@student.kuleuven.be

1. INTRODUCTION

Polyurethane (PU) foams represent an important and long-established class of polymeric materials for their mechanical, thermal, and acoustic properties. Lightweight PU foams are widely used as absorbing materials in various automotive applications (see Figure 1), because of their sound and mechanical energy dissipation properties, which allow an excellent Noise, Vibration and Harshness (NVH) comfort levels [1].

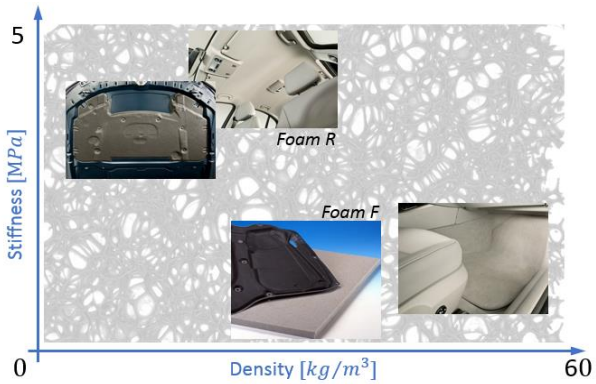

Figure 1. Properties' matrix of lightweight PU foams for automotive applications.

The high flexibility of PU chemistry, based on urethane reaction of isocyanate and polyol to form a structure-like polymer, allows to obtain PU foams, which can be either glassy or elastomeric at room temperature [2]. PU foams are characterised by a porous random microstructure, composed of a viscoelastic frame structure with air filling the voids. PU acoustic foams have often partially-open cells, in which cell faces are partially covered by thin membranes, which could influence the viscous-thermal dissipation as well as the elastic properties in foams [3]. The effect of cell face membranes has been recently analysed in [4, 5].

The energy transport within PU foams is carried through both the air-borne flow in the pores and the structure-borne vibration transmission. Several techniques have been developed to study the vibro-acoustic problems of porous materials. The first type, i.e. equivalent fluid models, considers the solid frame of the material to be rigid or limp such that a single longitudinal wave can propagate in the medium and therefore the acoustic properties depend on the effective density and the effective bulk modulus of the fluid. Such an assumption remains valid as long as the wave length is much larger than the pores' characteristic dimension and the fluid is considered incompressible. For simplicity reasons, empirical models are still widely used, but only a few acoustic parameters can be directly derived from them [6]. For this reason, they are not used in this work. Conversely, phenomenological models consider the wave propagation inside the pores at a microscopic level. The viscous and thermal losses can be related at the macroscopic level to five geometrical parameters: the open porosity ϕ, the static airflow resistivity σ_0, the tortuosity α_∞, the viscous Λ_{vis} and the thermal Λ_{thm} characteristic lengths. Although equivalent fluid models are widely used in the literature to model acoustic porous materials [7-9], they do not consider the vibrations of the foam's microstructure and therefore they do not allow to study the coupled mechanical and acoustic wave propagation occurring e.g. in PU flexible foams. The second type, i.e. poroelastic models, which considers the solid phase as elastic characterised by a mass and a stiffness, and allows a shear and two compressional waves to propagate, can therefore be used to overcome equivalent fluid models' limitations. The principal coupling theory is the Biot model [10, 11], which links the macroscopic fluid and solid displacement fields with the fluid effective parameters.

The vibro-acoustic characterisation of PU foams is of fundamental importance to predict and compare the NVH comfort levels of different materials and eventually to improve the microstructural design by adjusting the chemical formulation. Some parameters, e.g. ϕ, σ_0 and the surface acoustic impedance Z, can be directly measured without great difficulties, whereas others are usually more complex to measure without ultrasonic techniques [12]. For that reason, in this work, the inverse calculation of acoustic parameters based on impedance tube data has been employed. First, Attenborough, Wilson and Johnson–Champoux–Allard's (JCA) equivalent fluid models for wave propagation in porous materials have been used to analyse the acoustic behaviour of a rigid absorbing PU foam. The motionless solid frame does not allow the usage of equivalent fluid techniques to study the vibro-acoustic behaviour of flexible PU foams, characterised by a soft-like microstructure. For that reason, the Biot poroelastic model has been applied in its one-Dimensional (1D) form to find the mechanical and acoustic parameters of a flexible absorbing PU foam, by considering the interaction of elastic frames and the fluid in pores.

2. MODELLING SOUND PROPAGATION IN POROUS MATERIAL

This section presents an overview of the models for wave propagation in porous materials used in this paper. First, a brief explanation of equations governing equivalent fluid models is presented. Second, the expressions of the effective density ρ_{eq} and the effective bulk modulus K_{eq} obtained with Attenborough's extended cylindrical pore models, Wilson and JCA's phenomenological models, are introduced. Finally, the Biot poroelastic model is briefly presented.

The phenomenological and poroelastic models assume the validity of the homogenization long-wavelength condition, i.e. $L \gg l$ being L and l the macroscopic and the microscopic sizes of the Representative Volume Element (RVE), defined as the smallest volume of porous material representative of the whole [7].

2.1 Equivalent Fluid Models

Equivalent fluid models assume that the fluid within the pores does not excite the material structures; in other words, the skeleton can be assumed as motionless. This assumption is valid if the stiffness and/or the density of material structures are larger than that of the air and the wavelength is much larger than the characteristic dimension of the pores [13]. If these conditions are met, the propagation of the sound can be described by an equivalent fluid with a $\rho_{eq}(w)$ and a $K_{eq}(w)$, being ω the angular frequency. Such problem is governed by the Helmholtz equation:

$$\nabla^2 p_{eq} + k_{eq}^2 p_{eq} = 0 \tag{1}$$

where p_{eq} is the acoustic pressure and k_{eq} the frequency dependent wave number, defined as:

$$k_{eq} = w\sqrt{\frac{\rho_{eq}(w)}{K_{eq}(w)}} \tag{2}$$

The specific characteristic acoustic impedance Z_c can then be calculated as:

$$Z_c = \frac{\sqrt{\rho_{eq}(w)K_{eq}(w)}}{\rho_0 c_0} \tag{3}$$

where ρ_0 is the density of the air and c_0 is the sound velocity in the air. Restricting the formulation to the case of an impedance tube where a foam sample, i.e. layer of equivalent

fluid, is in contact on one side with the air, i.e. second layer of fluid, and, on the other side, is backed by a rigid wall, the specific acoustic impedance Z is given by [7]:

$$Z = -iZ_c \cot(k_{eq}(w)t) \tag{4}$$

where t is the sample thickness, i is the imaginary unit and cot is the cotangent function. Z can be related to the sound absorption coefficient α through the reflection coefficient R, defined as the ratio of the pressures p' and p created by the outgoing and ingoing waves at the layer surface.

$$Z = \frac{1+R}{1-R} \tag{5}$$

$$\alpha = 1 - |R|^2 \tag{6}$$

2.1.1 Extended cylindrical pore models (*Attenborough*)

Attenborough [14], extending Zwikker and Kosten's [13] theory, described the wave propagation in porous materials including viscous and thermal effects, to consider the anisotropic nature of pores. He adapted the expressions of $\rho_{eq}(w)$ and $K_{eq}(w)$ to include the tortuosity α_∞ and the shape factor b, assumed equal to 1 in this work, i.e. cylindrical pores. The adapted expressions are therefore given by:

$$\begin{cases} \rho_{eq}(w) = \dfrac{\rho_0 \alpha_\infty}{1 - \dfrac{2J_1(s'\sqrt{-i})}{s'\sqrt{-i}J_0(s'\sqrt{-i})}} \\ K_{eq}(w) = \dfrac{P_0 \gamma}{1 + \dfrac{(\gamma-1)2J_1(s'\sqrt{-iPr})}{s'\sqrt{-iPr}J_0(s'\sqrt{-iPr})}} \end{cases} \tag{7}$$

where P_0 is the ambient air pressure, γ is the ratio of specific heat capacity of the air, Pr is the Prandtl number, J_0 and J_1 are Bessel functions of the first kind of order 0 and 1 and s' is given by:

$$s' = b\sqrt{\frac{8w\rho_0\alpha_\infty}{\sigma_0\phi}} \tag{8}$$

where ϕ is the open porosity and σ_0 the static airflow resistivity.

Despite its simplicity, Attenborough's model is not ideal for this study as it allows to determine only two material parameters, σ_0 and α_∞. Moreover, the random microstructure of PU foams cannot be oversimplified by uniform cylindrical pores.

2.1.2 Phenomenological models

Phenomenological models consider the wave propagation problem on a microscopic level and wave propagation inside the pore networks is therefore included in the study. Readers can refer to [7] for a good overview of the main phenomenological methods and their formulation.

Johnson-Champoux-Allard model (*JCA*)

JCA model allows a better description of the wave propagation than Attenborough's one, considering both the viscous and thermal effects in arbitrary-shaped pores [15]. JCA model accurately describes the wave propagation process mainly at medium and high frequency ranges. The expressions of $\rho_{eq}(w)$ and $K_{eq}(w)$ are given by:

$$\begin{cases} \rho_{eq}(w) = \rho_0 \alpha_\infty \left(1 + \dfrac{\sigma_0 \phi}{i \rho_0 w \alpha_\infty} \sqrt{1 + \dfrac{4 i \alpha_\infty^2 \eta \rho_0 w}{\sigma_0^2 \Lambda_{vis}^2 \phi^2}}\right) \\ K_{eq}(w) = \dfrac{P_0 \gamma}{\gamma - (1-\gamma) \Big/ \left(1 + \dfrac{8\eta}{i w \rho_0 \mathrm{Pr}^2 \Lambda_{thm}^2} \sqrt{1 + \dfrac{i w \rho_0 \mathrm{Pr}^2 \Lambda_{thm}^2}{16 \eta}}\right)} \end{cases} \tag{9}$$

where η is the dynamic viscosity of the air, Λ_{vis} and Λ_{thm} are the viscous and thermal characteristic lengths of the material, respectively. More advanced formulations of JCA model, which consider more parameters, can be found in [16, 17].

Wilson model (*Wilson*)

By characterizing viscous and thermal effects as relaxation processes, Wilson proposed a model aiming at the mid-frequency range behaviour of porous materials [18]; indeed, such model lacks the asymptotic behaviour in very low and high frequencies. The expressions of $\rho_{eq}(w)$ and $K_{eq}(w)$ are given by:

$$\begin{cases} \rho_{eq}(w) = \dfrac{\rho_0 \alpha_\infty}{\phi} \dfrac{\sqrt{(1 + i w \tau_{vor})}}{\sqrt{(1 + i w \tau_{vor})} - 1} \\ K_{eq}(w) = \dfrac{P_0 \gamma}{\phi} \dfrac{\sqrt{(1 + i w \tau_{ent})}}{\sqrt{(1 + i w \tau_{ent})} + \gamma - 1} \end{cases} \tag{10}$$

where τ_{vor} and τ_{ent} are the vorticity- and entropy-mode relaxation times, respectively, given by:

$$\tau_{vor} = \frac{2 \rho_0 \alpha_\infty}{\phi \eta} \quad \tau_{ent} = \tau_{vor} Pr \tag{11}$$

The vorticity-mode relaxation time is characterised by a velocity field with non-vanishing rotation, in which the pressure and the velocity are involved, while the entropy-mode relaxation time is characterised by the heat exchange to which the entropy, the temperature and the density are related.

2.2 Poroelastic Model (*Biot*)

Poroelastic models consider the solid phase as an elastic material, characterised by a Young's modulus E, a Poisson ratio ν and a damping loss factor η_l; the mutual interaction between the solid frames and the fluid in pores is therefore analysed. Among poroelastic models, a central place is given to Biot theory [10, 11, 19]. Assuming no dispersion of the velocity in the elastic solid structures and wavelengths much larger than the dimensions of RVE, Biot developed a Lagrangian model to derive the stress-strain relations in solid ($\sigma_{ij}^s, \varepsilon_{ij}^s$) and fluid ($\sigma_{ij}^f, \varepsilon_{ij}^f$) domains from a potential energy of deformation by considering the contribution of the frame Θ^s and the air Θ^f dilatations to the stress filed, according to:

$$\begin{aligned} \sigma_{ij}^s &= [(P - 2N)\Theta^s + Q\Theta^f]\delta_{ij} + 2N\varepsilon_{ij}^s \\ \sigma_{ij}^f &= (-\phi p)\delta_{ij} = (Q\Theta^s + R\Theta^f)\delta_{ij} \end{aligned} \tag{12}$$

In Equation 12, N, P, Q and R are elastic coefficients which, assuming an incompressible frame' material, are given by:

$$\begin{cases} N = \dfrac{E(1+i\eta_l)}{2(1+\nu)} \\ P = 2N\dfrac{1-\nu}{1-2\nu} + \dfrac{Q^2}{R} \\ Q = (1-\phi)K_{eq} \\ R = \phi K_{eq} \end{cases} \tag{13}$$

K_{eq} is the frequency-dependent effective bulk modulus of the fluid, given by Equations 7, 9 or 10. JCA model, i.e. Equation 9, is used in this work.

The two compressional waves and the shear wave can therefore be known, and the characteristic impedance related to the wave propagation can eventually be derived from the macroscopic displacements of the frame and the air. The computation of wave propagation in the 3D space using the Biot theory usually requires computer aided engineering tools. However, the study of this paper is limited to the sound wave propagation occurred during acoustic measurements in an impedance tube, and therefore the 1D analytical solution of the Biot theory can be used. Readers can refer to [7] for the complete formulation of the Biot theory.

3. MATERIALS

In this work, a rigid sound absorbing foam (hereafter called Foam R) and a flexible sound absorbing foam (Foam F) are studied. The two materials are taken as representatives of the two main classes of industrial sound absorbing PU foams. Cylindrical samples of different thicknesses, i.e. $t = 2, 3, 4$ *cm*, are considered to investigate the influence of the sample's geometry on the acoustic absorbing performance and to further improve the parameters' optimization using simultaneously datasets from samples of different thicknesses. Table 1 reports the geometrical and the material properties. σ_0 is directly measured by monitoring the pressure drop across the sample with respect to the volumetric flow rate [20].

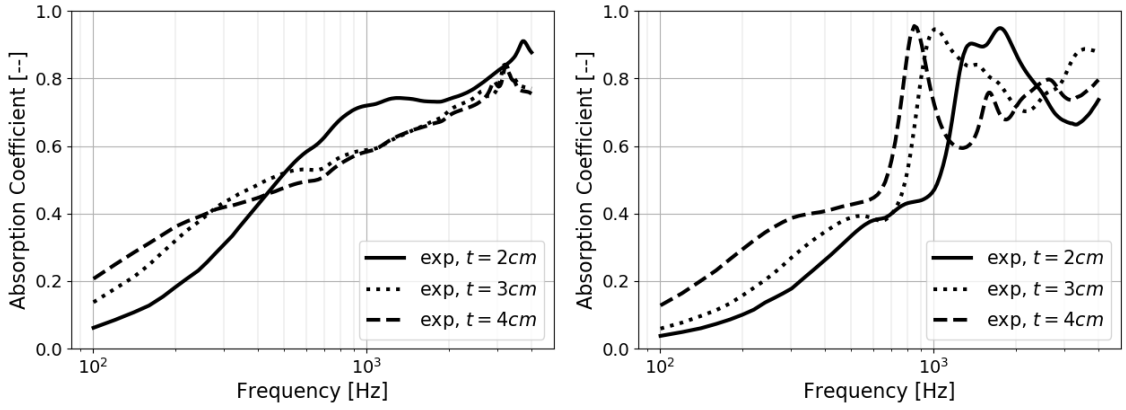

Figure 2. Sound absorption coefficient α of Foam R (left column) and Foam F (right column) cylindrical samples with $t = 2, 3, 4$ cm, measured with an impedance tube.

Figure 2 shows sound absorption coefficients α of Foam R and F, measured using an impedance tube [21, 22]. The incoming and outcoming sound signals are detected by the two microphones over 100-4000 *Hz* frequency range. Increasing the foam thickness, the general absorbing performances of foams at low frequency range improve. The α-curves of foam F show a major slope change in the frequency range between 400-800 *Hz*, due to elastic micro-resonances of flexible structures.

Figure 3 shows the mastercurves of the storage modulus for Foam R and F at 20 ℃, obtained from Dynamic Mechanical Analysis (DMA) data. All the measurements are performed with a Q800 testing machine by TA, applying a nominal sinusoidal strain of about 0.6 % with a frequency swept between 0.1 and 10 *Hz*, varying the temperature from −75 ℃ to 120 ℃. Details on the mastercurve calculation can be found in [23]. These DMA results show clearly the very different polymer stiffness of Foam R, i.e. stiff material, compared to that of Foam F, i.e. compliant material, in the small-strain viscoelastic regime.

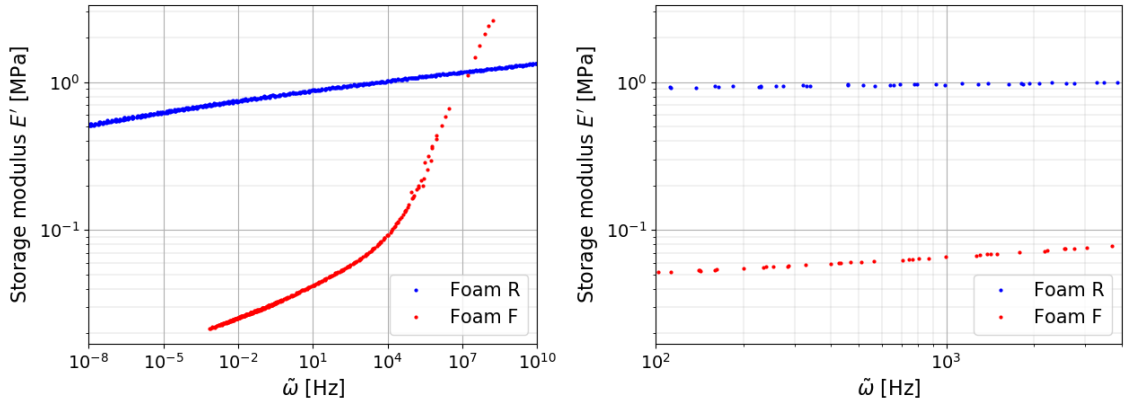

Figure 3. Mastercurves of Foam R and Foam F at 20℃, obtained from the DMA.

Micro-CT (μCT) scans with a Bruker Skyscan 1272 at a resolution of 5.4 μm are performed for foam R and F. 3D reconstructions and image analyses are made using Bruker's NRecon and CTAn software, while cell size analysis is made using in-house developed code. Image analysis involves creating fully connected skeleton structures of scanned data of foam samples. This is done by segmenting the data into air pores and solid structures. From these skeleton structures, it is possible to calculate the sizes of the air pores and the solid structures in the microstructures. The microstructure, coloured with cell size, and the pores size distributions of Foam R and F are shown in Figure 4; Foam F has a larger average cell diameter (546.7 μm) than that of Foam R (450.3 μm) and a more polydisperse microstructure.

Table 1. Geometrical and material properties of Foam R and Foam F.

	Foam R	**Foam F**
Thicknesses, t $[mm]$	21.9, 32.1, 42.7	21.7, 30.4, 42.6
Diameter $[mm]$	44.5 + [0.08]	44.6 + [0.10]
Density, ρ $[kg/m^3]$	21.6 + [0.37]	26.2 + [0.39]
Porosity, ϕ [-]	98.1% + [0.03]	97.6% + [0.04]
Flow resistivity, σ_0 $[kNs/m^4]$	68.6 + [12.7]	54.3 + [7.31]

4. ALGORITHM

In Section 2, Z has been analytically related to both acoustic and elastic parameters through different models. Hence, a non-linear regression fit can be implemented to identify such parameters using the direct measurements of Z for Foam R and F. The cost function is therefore the residue between the experimental data Z_{exp} and the one predicted by the different models. Parameters' bonds are used to limit the searching domain; α_∞ is constrained to be greater than 1, i.e. parallel streamlines of the velocity field, and lower

than 10 [8]. Λ_{vis} must be smaller than Λ_{thm} as the former is defined as the interconnection between pores and the latter is linked to pore sizes [9].

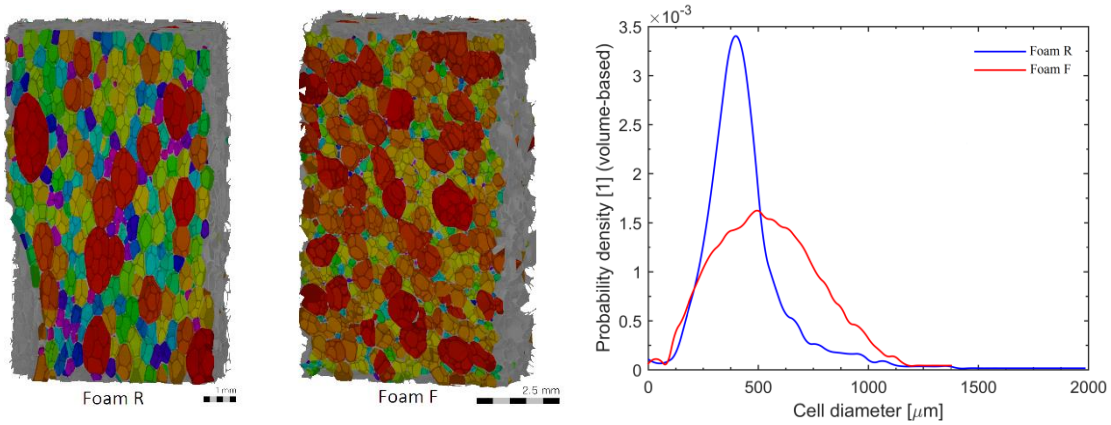

Figure 4. Individual foam cell reconstruction, coloured with cell size (left column) and pore size distribution of Foam R and Foam F (right column).

To increase the fitting accuracy, several authors [9] proposed a separate fitting of different areas of the α-curve, i.e. a low-frequency one where α increases rapidly, a medium-frequency one where α has a peak and a high-frequency one where α tends to be stable. However, the main drawback of such approach is that to obtain different acoustic parameters for the same sample, losing their consistent physical meanings and connection to foam materials. In this context, curves obtained from samples of different thicknesses are fitted simultaneously to the entire analysed frequency range, in order to derive a unique and physically valid group of material parameters.

5. RESULTS AND DISCUSSION

Figure 5 shows the comparison between measured values of Z and α, and predicted ones using the equivalent fluid inverse methods, based on Attenborough, JCA and Wilson models for the cylindrical sample of Foam R with $t = 2\ cm$. Table 2 reports the values of obtained acoustic parameters and the corresponding error, calculated as the mean squared error of α. The results of these three models are all satisfactory and the identified parameters are close to each other. Nevertheless, σ_0 is generally slightly overestimated compared with values measured; however, Wilson model gives the closest estimation, which is included in the measurements' range.

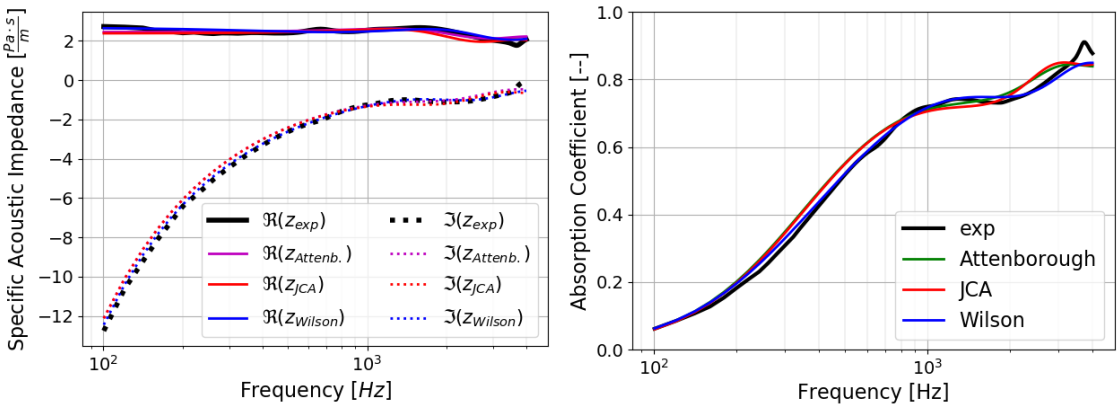

Figure 5. Foam R: comparison between measured and predicted values of Z (left column) and α (right column) for a cylindrical sample with $t = 2\ cm$.

Table 2. Foam R: acoustic parameters calculated with inverse methods based on Attenborough, JCA and Wilson models for a cylindrical sample with $t = 2$ cm. Wilson ($multi_t$) fitting algorithm employs simultaneously datasets of samples with $t = 2, 3, 4$ cm.

	α_∞	$\Lambda_{vis}[\mu m]$	Λ_{thm} $[\mu m]$	σ_0 $[kNs/m^4]$	**Error** [%]
Attenborough	3.8	--	--	91.6	2.9
JCA	3.4	54	196.7	92.1	3.1
Wilson	2.9	42.6	201.1	80.9	3.5
Wilson ($multi_t$)	3.4	38.4	233.9	94.7	4.8

Although Attenborough model has the advantage to be simple to implement, it allows to calculate only α_∞ and σ_0. Conversely, JCA model predicts a large number of acoustic parameters, describing with a high accuracy the wave propagation process mainly at medium and high frequency ranges. Its mean squared error at low frequency $[0.1: 1]$ *kHz* (8.8 %) is much higher than that of Wilson (2.5 %). Indeed, the JCA asymptotic formulation does not require the imaginary part of dynamic permeability to exactly satisfy its frequency dependence for frequencies lower than the transition between viscous force-dominated flow and inertial force-dominated flow [7].

PU foams are characterised by a porous random microstructure, which contributes to produce anisotropic and/or spatially-dependent material properties. Moreover, the fitting parameters are very sensitive to the initial data and therefore to the sample measured. To obtain more reliable values of acoustic parameters, a fitting process employing simultaneously different datasets of samples with $t = 2, 3, 4$ *cm* is implemented. In this case, Wilson model is used due to its simplicity and its low error over the entire frequency range. Figure 6 shows that parameters obtained using Wilson model employing different datasets can predict with a good accuracy (see Table 2) the α-curves for all samples analysed. An additional verification of the results' accuracy can be implemented to link some macroscopic parameters to the analysis of the foam microstructure obtained with μCT. Indeed, according to [7], $2\Lambda_{thm}$ is representative of the material's pore size. In this case, Wilson ($multi_t$), which uses different thickness datasets, gives the more representative values of acoustic parameters ($2\Lambda_{thm} = 466\ \mu m \approx 450\ \mu m$).

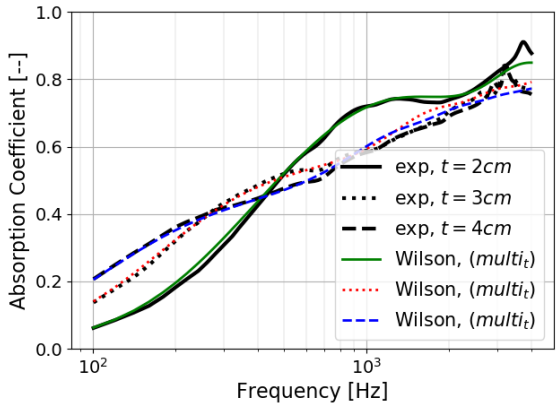

Figure 6. Foam R: comparison between measured and predicted values of α obtained using Wilson model employing simultaneously different datasets of samples with t=2, 3, 4 cm.

Equivalent fluid models can describe accurately the wave propagation within PU rigid absorbing materials, like Foam R, because the assumption of the motionless solid frame remains valid. However, several PU foams, like e.g. Foam F, are elastomeric at room temperature, characterised by an elastic frame. For such class

of foams, equivalent fluid models cannot fully characterise the vibro-acoustic behaviour. Indeed, Figure 7 shows the poor prediction of Z and α (see blue curves), obtained with parameters fitted with Wilson model, especially around the resonances of the structures at low frequency range.

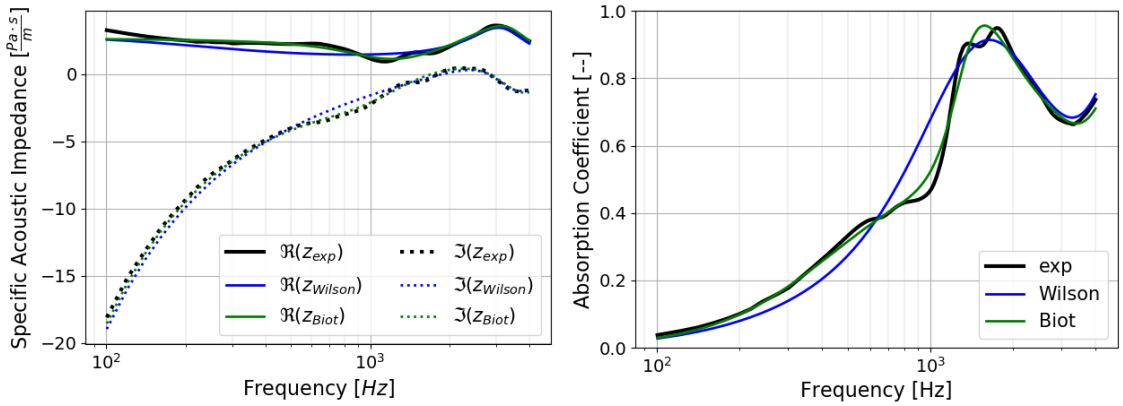

Figure 7. Foam F: comparison between measured and predicted values of Z (left column) and α (right column) of a sample with $t = 2$ cm, obtained with Wilson equivalent fluid model and Biot poroelastic model.

For that reason, the poroelastic inverse method based on Biot theory coupled with the JCA model is more appropriate to better characterise the wave propagation process within Foam F, see Figure 7 (green curves). Conforming to what was done for Foam R, Figure 8 (left column) shows the comparison between measured and predicted values of α obtained with the Biot model employing simultaneously different datasets of samples with $t = 2, 3\ cm$. The acoustic parameters obtained are therefore more representative of the heterogeneity of Foam F (see Table 3).

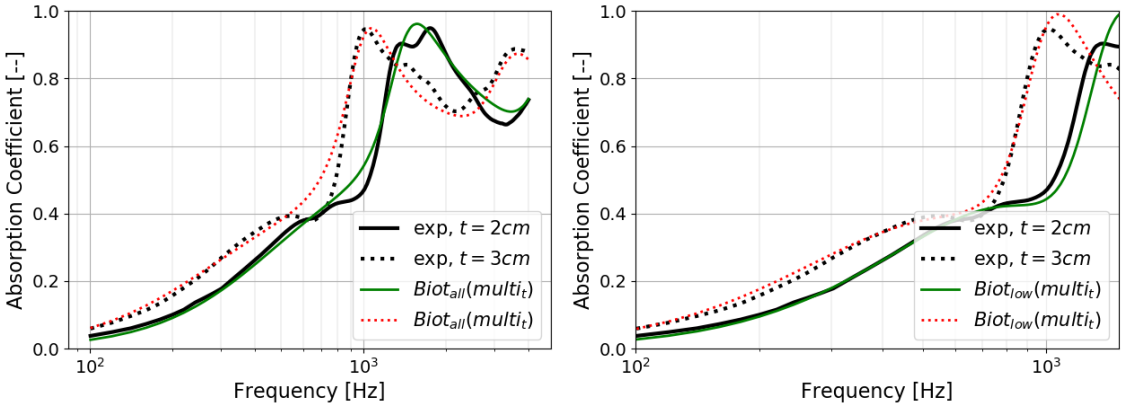

Figure 8. Foam F: comparison between measured and predicted values of α obtained with Biot model employing simultaneously datasets of different samples with t=2, 3 cm, and fitting the data in $[0.1; 4]$ *kHz (left column) and* $[0.1; 1]$ *kHz (right column) frequency ranges.*

Since the Biot theory can describe structures' resonances, a closer look on $[0.1: 1]$ *kHz* frequency range is taken by fitting the data in this range using Biot model for datasets of different thicknesses. Figure 8 demonstrates that the predicted curves fit well in such frequency range, obtaining at the same time reasonable values of acoustic parameters (see Table 3). Values of Young's modulus are similar to those found in DMA results (see Figure 3), demonstrating the validity of the fitting algorithm to describe the poroelastic behaviour of Foam F. In this case, correlation between Λ_{thm} and the foam microstructure analysis obtained with μCT (see Figure 4) is less accurate than that of Foam R. This can

be explained by the more polydisperse microstructure of Foam F, which gives a broader pore size distribution. Results are therefore more sample-dependent.

Table 3. Foam F: acoustic parameters of a sample with $t = 2$ cm, calculated using the Biot model, fitting the data in $[0.1; 4]$ *kHz* ($\mathbf{Biot}_{all}$) *and* $[0.1; 1]$ *kHz* ($\mathbf{Biot}_{low}$) *frequency ranges. Wilson* ($multi_t$) *algorithm employs simultaneously datasets of samples with* $t = 2, 3$ *cm.*

	$\boldsymbol{\alpha_\infty}$	$\boldsymbol{\Lambda_{vis}}[\mu m]$	$\boldsymbol{\Lambda_{thm}}$ $[\mu m]$	**E** [kPa]	$\boldsymbol{\nu}$	$\boldsymbol{\eta}$	$\boldsymbol{\sigma_0}$ $[kNs/m^4]$	**Error** [%]
$\mathbf{Biot}_{all}(t = 2\ cm)$	2.1	17.8	175.3	71.2	0.44	0.44	116.6	3.1
$\mathbf{Biot}_{low}(t = 2cm)$	3.8	25.7	233.6	204.5	0.32	0.31	69.6	8.7
$\mathbf{Biot}_{all}(multi_t)$	3.7	68.8	97.3	104	0.28	0.43	115.6	3.4
$\mathbf{Biot}_{low}(multi_t)$	3.8	39.3	203.1	194	0.28	0.24	75.5	2.9

6. CONCLUSIONS

In this work, acoustic parameters of a flexible and a rigid sound absorbing foam were derived through an inverse calculation based on direct impedance tube measurements.

Equivalent fluid models (Attenborough, JCA and Wilson), based on the assumption of a motionless solid frame, were compared to a poroelastic method based on the Biot theory coupled with the JCA model, which considered the interaction between the elastic frames and the fluid within pores, to characterise the acoustic behaviour of PU foams. Results have shown that former methods yielded accurate results for the rigid sound absorbing foam, whereas the latter method provided a unique group of acoustic parameters, which is able to describe the acoustic behaviour of the flexible sound absorbing foam, characterised by soft-like polymeric structures.

To improve the models' reliability and their ability to represent the random microstructure of PU foams, an inverse calculation that simultaneously fitted impedance tube results from samples with different thicknesses, was proposed. In addition, the entire frequency range was analysed simultaneously, to maintain a clear physical meaning of the acoustic parameters. This yielded a comparable accuracy level, i.e. mean squared error less than 5%, to that of those approaches fitting separately each area of α-curves. Moreover, a good correspondence was found between certain macroscopic properties obtained by the inverse calculations and the analysis of the material microstructure obtained with μCT. Indeed, algorithms using datasets of different thicknesses gave accurate values of acoustic parameters for the analysed PU foams.

7. ACKNOWLEDGEMENTS

The authors would like to thank Jan Lauwers, Joris Pittevils, Luc Van Essche and Philip Berthels for providing the PU absorbing foam samples, Rajesh Gajendran for static airflow measurements and Kristof Verniers and Rene Boonen for fruitful discussions on sound absorption measurements.

8. REFERENCES

1. C. Skinner, J. Peters and J. Vandenbroeck, *"Acoustic absorbers: a third way for the management of sound in automobiles"*, UTECH Europe, 28-30 March, Maastricht, Netherlands (2006).
2. D. Randall and S. Lee, "*The Polyurethanes Handbook"*, London: Wiley (2002).
3. M. T. Hoang and C. Perrot, "*Solid films and transports in cellular foams*", J. Appl. Phys., vol. 112, no. 5 (2012).

4. F. Chevillotte, C. Perrot and E. Guillon, "*A direct link between microstructure and acoustical macro-behavior of real double porosity foams*", J. Acoust. Soc. Am., vol. 134, no. 6, pp. 4681-4690 (2013).
5. M. Brennan, M. Dossi, M. Moesen, "*A Multi-Physics Study of the Wave Propagation Problem in Open Cell Polyurethane Foams*", Comsol Conference, 18-20 October, Rotterdam (2017).
6. M. E. Delany and E. N. Bazley, "*Acoustical properties of fibrous materials*", Applied Acoustics, vol. 3, pp. 105-116 (1970).
7. J. F. Allard, "*Propagation of sound in porous media: modeling sound absorbing materials*", Elsevier Applied Science. New York (2009).
8. Y. Atalla and R. Panneton, "*Inverse acoustical characterization of open cell porous media using impedance tube measurements*", Canadian Acoustics, vol.33, no.1, pp. 11-24 (2005).
9. K. Verdiere, N. Atalla and R. Panneton, "*A case study of full inverse poroelastic characterization of an open-cell porous material using an impedance tube: the need to properly prepare the material and to control the measurement*", SAE Technical Paper, ref: 2018-01-1567 (2018).
10. M. A. Biot, "*Theory of propagation of elastic waves in a fluid-saturated porous solid. i. low-frequency range*", J. Acoust. Soc. Am., vol. 28, no. 2, pp. 168-178 (1956).
11. M. A. Biot, "*Theory of propagation of elastic waves in a fluid-saturated porous solid. ii. high-frequency range*", J. Acoust. Soc. Am., vol. 28, no. 2, pp. 179-191 (1956).
12. P. Leclaire, L. Kelders, W. Lauriks, C. Glorieux, and J. Thoen, "*Determination of the viscous characteristic length in air-filled porous materials by ultrasonic attenuation measurements*", Acoust. Soc. Am., vol. 99, no. 4, pp. 1944-1948 (1998).
13. C. Zwikker and C.W. Kosten. "*Sound absorbing materials*", Elsevier, New York (1949).
14. K. Attenborough, "*Acoustical characteristics of rigid fibrous absorbents and granular Materials*", J. Acoust. Soc. Am., vol. 73, no. 3, pp. 785-799 (1983).
15. J. F. Allard and Y. Champoux, "*New empirical equations for sound propagation in rigid frame fibrous materials*", J. Acoust. Soc. Am., vol. 91, no. 6, pp. 3346-3353 (1992).
16. D. Lafarge, P. Lemarinier, J. F. Allard, and V. Tarnow, "*Dynamic compressibility of air in porous structures at audible frequencies*". J. Acoust. Soc. Am., vol. 102, pp. 1995-2006 (1997).
17. S. R. Pride, F. D. Morgan, and F. A. Gangi, "*Drag forces of porous-medium acoustics*", Phys. Rev. B, vol. 47, no. 9, pp. 4964-4975 (1993).
18. D. K. Wilson, "*Relaxation-matched modeling of propagation through porous media, including fractal pore structure*", J. Acoust. Soc. Am., vol. 94, pp. 1136-1145 (1993).
19. Y. Champoux and J. F. Allard, "*Dynamic tortuosity and bulk modulus in air-saturated porous media*", J. Appl. Phys., vol. 70, no. 4, pp. 1975-1979 (1991).
20. ISO 9053, "*Acoustics – Materials for acoustical applications – Determination of airflow resistance"*, International Standards Organization, Geneva (1991).
21. ISO 10534-2, "*Acoustics-Determination of sound absorption coefficient and impedance in impedance tubes. 2. Transfer-function method*", International Standards Organization, Geneva (1998).
22. R. Boonen, P. Sas, W. Desmet, W. Lauriks and G. Vermeir, "*Calibration of the two-microphone transfer function method to measure acoustic impedance in a wide frequency range*", Proceedings of the International Conference on Noise and Vibration Engineering, vol. 1, pp. 4501-4511, Leuven, Belgium (2006).
23. A. Opreni, S. Mariani, M. Dossi and M. Brennan, "*Combined Effects of Temperature and Humidity on the Mechanical Properties of Polyurethane foams*", J. Rheol, submitted (2019).